JOURNAL OF OPTOELECTRONICS AND ADVANCED MATERIALS Vol. 9, No. 1, January 2007, p. 1 - 10

Georgi Nadjakoff Memorial Lecture

Progress in the science and technology of direct conversion X-ray image detectors: The development of a double layer a-Se based detector

S. O. KASAP*, G. BELEV
Department of Electrical and Computer Engineering, University of Saskatchewan, Saskatoon, S7N 5A9, Canada

One very important requirement for an X-ray photoconductor to be usable in a practical detector is that the dark current at the operating field should be as low as possible. We examine, in terms of an order of magnitude calculations, the maximum allowed dark current density, which is ~10 pA mm^{-2}. Dark currents in presently competing X-ray photoconductors are compared and discussed. We pay particular attention to a-Se based photoconductors inasmuch as the progress in the science and technology of a-Se based detectors has led to their commercialization. We report and discuss dark current measurements on single and double layer a-Se based photoconductor structures, and show how these measurements paved the way to the development of a new a-Se based X-ray detector fabricated on a CCD that is suitable for slot scanned X-ray imaging. The a-Se CCD detector has provided excellent images, and has a remarkable high resolution, better than 16 lines mm^{-1}.

(Received November 2, 2006; accepted December 21, 2006)

Keywords: X-ray photoconductors, X-ray detectors, a-Se alloys, Dark current, a-Se, HgI_2, PbO, CdZnTe

1. Introduction

Direct conversion flat panel X-ray image detectors have been reviewed in the literature by Rowlands and co-workers, in terms of their principles of operation, performance, limitations, and the photoconductors that can be used in the direct conversion [1,2].

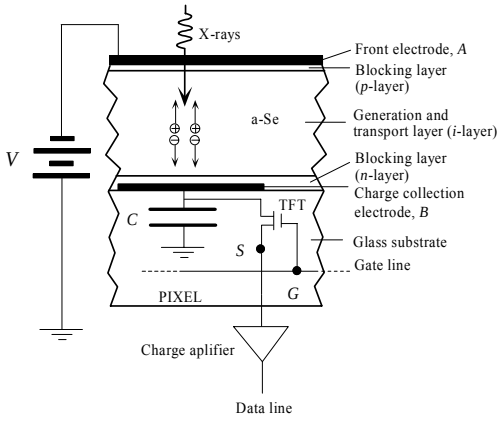

Fig. 1. The schematic diagram of one of the pixels in a direct conversion flat panel X-ray image detectors.

A flat panel X-ray image detector is essentially a large area integrated circuit that is able to capture an X-ray image and convert it to a digital form for image display, analysis and storage. Such flat panel detectors can replace the X-ray film/screen cassettes of today, and thereby provide a smooth transition to digital radiography. The flat panel image detector consists of millions of pixels each of which acts as an individual detector as shown schematically in Fig. 1 for a particular type of detector that uses a-Se as the photoconductor. Each pixel converts the radiation it receives to an amount of charge proportional to the incident radiation.

There are two methods of conversion, direct and indirect. In a *direct conversion detector*, X-rays are absorbed in a photoconductor (such as a-Se) and generate charges that drift through the conductor and become collected on a storage capacitor *C* as shown in Fig. 1. The collected charge *Q* on the capacitor *C* then constitutes the signal. At an appropriate (access) time, the thin film transistor (TFT) is activated and turns on to pass the charge *Q* on *C*, over an interconnect line, to a charge amplifier, which feeds the charge to the data line as a voltage signal. In the particular example in Fig. 1, the a-Se photoconductor has thin blocking layers, called *p*- and *n*-layers, between the photoconductor and the metal electrode contacts to reduce the dark current due to injection from the contacts [3]. The triple layer structure for the a-Se photoconductor is called a *pin* structure for reasons described and discussed later in the paper.

In indirect conversion, the X-rays are first absorbed in a phosphor medium, such as CsI_2, and become converted to light. There is an a-Si *pin* photodiode at each pixel that detects the light emitted from the phosphor. This paper will consider only direct conversion flat panel X-ray imagers (DC FPXIs) and will review and discuss the progress in suitable photoconductors that can be used in such image detectors. We concentrate on a-Se based

photoconductors, since the progress in the science and technology of a-Se based detectors has led to their commercialization and use in various medical imaging modalities. One great advantage of a-Se based DC FPXIs is that they exhibit excellent resolution. Their presampling modulation transfer function, MTF, is almost identical to the theoretical MTF (sinc function) determined by the pixel aperture as shown by Hunt et al. [4].

A critical requirement for any detector is a sufficiently small dark current (I_d) that does not lead to an unacceptable performance in terms of degrading the signal to noise ratio (SNR) and hence the DQE (the detective quantum efficiency). We pay particular attention to dark currents in a-Se photoconductors and provide a new technology for fabricating an a-Se based double layer structure on a special CCD chip towards a new X-ray detector that can be used in slot scanning imaging. The new double-layer a-Se detector has a dark current that is comparable to, or lower than, the current commercial *pin* structures on the market, and has been shown to possess excellent resolution capabilities [5].

It may be thought that one can reduce the dark current by lowering the applied bias across the X-ray photoconductor. However, under a reduced field, the photoconductor operates with a charge collection efficiency $\eta_{\text{collection}}$ less than unity, and hence has a lower x-ray sensitivity. Good $\eta_{\text{collection}}$ implies that there should be no deep trapping of charge carriers as they drift through the photoconductor, so that the collected charge represents the actual charge that has been obtained by the x-ray-to-charge conversion process. If μ is the drift mobility, τ is the lifetime (with respect to deep trapping) of the drifting carriers, and if F is the applied field, then $\mu\tau F$ is the *schubweg* of the carriers, *i.e.* the average distance a carrier drifts before it is trapped. The term *range* usually refers to the $\mu\tau$ product, which is the distance drifted per unit field before the carrier is trapped.

One remarkable aspect of charge transport in many candidate photoconductors is the fact that we can describe the general transport behavior in terms of only two *effective* sets of traps (not necessarily located at discrete energy levels), shallow traps that modify the mobility μ, and deep traps that control the lifetime τ. For example, experiments carried out over several decades at Xerox and at the University of Saskatchewan clearly show that both hole and electron transport in a-Se can be described by shallow and deep traps [6-9]; and we can use two lifetimes τ_h and τ_e to represent the hole and electron deep trapping times. The use of shallow and deep traps to describe charge transport has been also applied to other photoconductors such as PbI_2, HgI_2 etc. The dependence of the sensitivity on the carrier ranges can be calculated by carrying out an analysis similar to the Hecht collection efficiency [10]. In general, x-ray radiation is absorbed throughout the bulk of the photoconductor, which means that the overall collection efficiency will be more complicated, but, nonetheless, computable. There are several examples in the literature with applications [11-13].

2. Dark currents

Since photoconductors are used under an applied bias, there is always a dark current I_d that flows in the sample. In a good photoconductor, the signal current is much larger than the dark current. We need to set an upper limit for the dark current that can be tolerated. We provide a straight forward order of magnitude estimate for the maximum I_d as follows.

We impose a negative bias on the radiation receiving electrode (as in Fig. 1), and take the photoconductor to have nearly perfect charge transport properties; we neglect recombination and trapping effects. We take the pixel area A to be roughly $(100\ \mu m)^2$. Suppose that N_o is the total number of electrons generated by the absorbed X-ray photons that we wish to detect. In medical imaging N_o would be in the range 10^3 to 10^5 electrons. The TFT samples the charge eN_o on the capacitor C every Δt seconds. Over a time Δt, the dark current density J_d accumulates $J_d A\Delta t/e$ electrons on C. There is a statistical variation in this collected charge that corresponds to $(J_d A\Delta t/e)^{1/2}$ electrons. We would like this fluctuation to be no more than the quantum noise in the signal N_o, which is $N_o^{1/2}$. Thus, we would like

$$(J_d A\Delta t/e)^{1/2} < N_o^{1/2}. \quad (1)$$

Taking $N_o \sim 10^3$ electrons, we obtain $J_d < 1.6\times10^{-12}$ A cm^{-2} or 0.016 pA mm^{-2}. The latter allowed dark current seems quite small because we have not considered other possible noise sources in the detection system. Under strong signals, the allowed dark current can be much larger. For $N_o \sim 10^5$ electrons, $J_d < 1.6\times10^{-10}$ A cm^{-2} or 1.6 pA mm^{-2}

One important noise mechanism is that associated with the reset or the switching action of the TFT switch shown in Fig. 1; it corresponds to thermal charge fluctuations in the circuit that contains C and the TFT. Even if the collected charge across C is zero, there will nonetheless be charge fluctuations across C as a result of the equipartition of energy in this system [14,15]. This noise is called reset or *kTC* noise and has been extensively studied [16]. Suppose that ΔQ is the instantaneous charge across C. Then, from the equipartition theorem, the average energy stored on C, $\langle\Delta Q^2\rangle/(2C)$ must be $kT/2$ where k is the Boltzmann constant and T is the temperature (300 K). Even if $\langle\Delta Q\rangle$ is zero, the mean squared fluctuation in ΔQ, $\langle\Delta Q^2\rangle$, would not be, which constitutes the *kTC* noise. In terms of fluctuations N_{reset} in the number of electrons, the above the *kTC* noise is equivalent to

$$N_{\text{reset}} = (kTC)^{1/2}/e \quad (2)$$

For such thermal fluctuations, the pixel and sample capacitances would be in parallel, though the sample capacitance is usually very small. C would typically be 0.5 – 2 pF, and we take C = 2 pF for the maximum dark current estimation. Generally, the reset noise is greater than the quantum noise in the signal. Thus we would like J_d to be not more than the reset noise,

$$(J_d A\Delta t/e)^{1/2} < (kTC)^{1/2}/e \quad (3)$$

for C = 2 pF, we need $J_d < 5\times10^{-10}$ A cm^{-2} or 5 pA mm^{-2}; and a smaller dark current if C is smaller.

One final consideration is the electronic noise in the read circuit. This is usually considered in terms of how many "noise" electrons it corresponds to, that is, the root mean square of the signal expressed as N_e number of electrons. N_e is usually 500 – 1000, and depends on the particular AMA and its peripheral electronics. We need to have the dark current such that $(J_d A\Delta t/e)^{1/2} < N_e$. Thus for $N_e \approx$ 500 - 1000 electrons, $J_d < 4\times10^{-10}$ A cm^{-2} or 4 – 16 pA mm^{-2}.

Given the order of magnitude calculations, and the independence of the noise sources that we have considered, it would be reasonable to expect the upper limit for the dark current to be of the order of 10 pA mm^{-2} for present DC FPXIs. The photoconductor design must achieve a dark current that does not far exceed this value. Later in this paper, we present a particular double layer a-Se based detector structure that does indeed achieve an acceptable level of dark current for the detector to be practically useful. Table 1 summarizes the upper limits to the dark current magnitudes, taking into account the above noise sources in the detector.

Table 1. C = 2 pF and pixel area A = (100 μm × 100 μm) N_o and N_e are the signal and electronic noise in the number of electrons respectively.

Noise	I_d (pA mm^{-2})
I_d noise < quantum noise $N_o = 10^3 – 10^5$ electrons	0.02 - 2
I_d noise < TFT reset noise	5
I_d noise < electronic noise N_e = 500 - 1000 electrons	4 - 16

It is should be emphasized that a better approach needs to consider the relationship between the dark current and the overall DQE of the detector, and also consider the minimum exposure that is needed for a given medical modality. It is likely that an acceptable level of DQE would correspond to $I_d < 10$ pA mm^{-2}.

Table 2 compares the present state of dark currents in various competing X-ray photoconductors for DC FPXIs. The dark current normally increases with the applied field. In the case of several polycrystalline photoconductors such as HgI_2, PbI_2, PbO *etc*, in order to keep the dark current at a tolerable level, one has to apply a small field, *e.g.* a field of 0.5 V/μm in the case of PVD polycrystalline HgI_2 yields a dark current of ~6 pA mm^{-2}. However, the charge collection efficiency at such low fields is poor; thus there is a reduction in the sensitivity due to an operation at a lower field. The case for PbI_2 is particularly acute, and demonstrates the interplay between keeping the dark current low and, at the same time, maintaining good charge collection efficiency. The dark current in a ITO/PbI_2/Pt is 10 pA mm^{-2} at a field of 0.3 V/μm. At the latter field, the charge collection efficiency is 0.3 [17].

Table 2. Dark current in various potential X-ray photoconductors. Data from [18]

Photoconductor, state, preparation	F V/μm	I_d pA/mm^2
Stabilized a-Se, Single layer	~10	< 10 up to 10 V/μm field
Stabilized a-Se, Multi layer (PIN or NIP)	~10	< 1 up to 20 V/μm field
HgI_2 Polycrystalline PVD	~0.5	~ 6 at 0.5 V/μm field
HgI_2 Polycrystalline SP	~1.0	~8 at 1.0 V/μm field
$Cd_{.95}Zn_{.05}Te$ Polycrystalline	~0.25	~25 at 0.25 V/μm field
PbI_2 Polycrystalline PVD	~0.5	10-50 at 0.5 V/μm field
PbO Polycrystalline	~1.0	40 at 3 V/μm field

3. Stabilized a-Se

Properties of various candidate X-ray photoconductors have been recently reviewed in reference [18]. The most developed X-ray photoconductor for DC FPXIs is still stabilized a-Se. Stabilized a-Se can be easily coated as thick films (e.g., 100-1000 μm) onto suitable substrates by conventional vacuum deposition techniques and without the need to raise the substrate temperature beyond 60-70 °C (much below the damage threshold of the AMA, e.g., ~300 °C for a-Si:H panels). Stabilized a-Se, not pure a-Se, is used in the X-ray sensors, because pure a-Se is thermally unstable and crystallizes over several weeks or months following manufacture. Crystalline Se is unsuitable as an X-ray photoconductor because it has a much lower dark resistivity and hence an orders of magnitude larger dark current than a-Se. Alloying pure a-Se with As (0.2 – 0.5% As) greatly improves the stability of the composite film and helps to prevent crystallization. However, it is found that the addition of As has an adverse effect on the hole lifetime because the arsenic introduces deep hole traps. If the alloy is doped with 10 – 20 parts per million (ppm) of a halogen (such as Cl), the hole lifetime is restored to its initial value. Thus, an a-Se film that has been alloyed with 0.2 – 0.5% As (nominal 0.3% As) is called stabilized a-Se. Stabilized a-Se may or may not be doped with Cl, depending on whether hole or electron transport is of interest. The density of a-Se is 4.3 g/cm^3 with an energy gap E_g = 2.0 - 2.2 eV.

The deep trap capture times or the lifetimes τ of carriers in a-Se vary substantially between different

samples and depend on various factors such as the source of the a-Se material, impurities, and the preparation method. The electron lifetime τ_e is particularly sensitive to impurities in the a-Se source material. The hole lifetime τ_h drops rapidly with decreasing substrate temperature, whereas the electron lifetime τ_e is independent of the substrate temperature [19]. Increasing the As concentration increases the electron range, whereas Cl doping increases the hole range [20]. Table 3 lists typical electron and hole ranges for stabilized a-Se photoconductors, along with those for competing X-ray photoconductors.

Table 3. Carrier ranges in various competing X-ray photoconductors. Data extracted from [18].

Photoconductor, state, preparation	Electron $\mu_e\tau_e$ (cm^2/V)	Hole $\mu_h\tau_h$ (cm^2/V)
Stabilized a-Se Vacuum deposition	0.3×10^{-6} - 10^{-5}	10^{-6} - 6×10^{-5}
HgI_2 Polycrystalline, PVD	10^{-5}-10^{-4}	~10^{-6}
HgI_2 Polycrystalline, screen printing	10^{-6}-10^{-5}	~10^{-7}
$Cd_{.95}Zn_{.05}Te$ Polycrystalline, Vacuum deposition	2×10^{-4}	3×10^{-6}
PbI_2 Polycrystalline, PVD	7×10^{-8}	2×10^{-6}
PbO Polycrystalline, Vacuum deposition	5×10^{-7}	–
TlBr Polycrystalline	–	1.5×10^{-6}

Amorphous Se has at least two distinct attributes in terms of its electronic properties. Firstly, in good quality material (electronic or xerographic grade) both holes and electrons are mobile and the material is effectively ambipolar. a-Se in which both electrons and holes are mobile has been coined "*i*-Se". Secondly, by appropriately doping a-Se, or changing the preparation conditions, one can control the carrier ranges, and thereby produce either *p*-type or *n*-type a-Se. The *p*-layer and *n*-layer terminology is different from that customarily used for semiconductors. Here the terms mean that they are appropriately doped to serve as unipolar conducting layers, which efficiently trap electrons (*p*-layers) or holes (*n*-layers) respectively, but allow the transport of the oppositely charged carriers. These *n*- and *p*-layers are used as blocking layers in commercial a-Se X-ray detectors to prevent carrier injection from the electrodes and thereby reduce the dark current as shown in Fig. 2. For example, the *n*-layer between the *i*-Se and the positive electrode would trap holes.

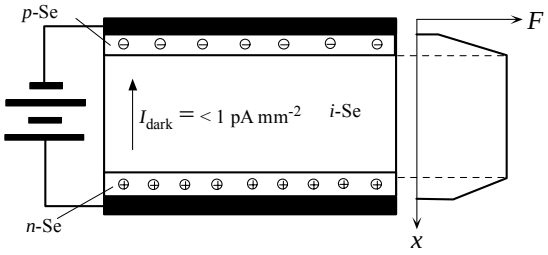

Fig. 2. The pin a-Se structure consists of thin n- and p-layers between the i-layer and positive and negative electrodes respectively. These n- and p-layers act as blocking layers against carrier injection into the i-layer.

The trapped holes in the *n*-layer decrease the field at the positive electrode, which reduces the hole injection rate. The rate of hole emission of these deeply trapped carriers is so small that there is no significant current injection into the bulk *i*-Se layer. Similar arguments apply to the *p*-layer which has trapped electrons which reduce the field at the negative electrode, and hence the electron injection rate from this electrode. The *n*- and *p*-layers thus act as "effective electrodes" that have finite thicknesses, and inject at an innocuous rate into the *i*-Se layer. By using *pin* structures, it has been possible to reduce the dark current to less than 1 pA/mm^2 at fields as high as 10 - 20 V/μm [3].

The success of the present commercial a-Se FPXIs is a direct result of the development of these *pin* structures that have very low dark currents.

4. Overview of dark currents in a-Se

The nature of the contacts to a-Se as an X-ray photoconductor is extremely important as ideally the dark current should be zero (as for any ideal photodetector). Although, during the sixties and seventies, many researchers reported *I-V* measurements on a-Se films, there has been no general conclusion on the behavior of metal/a-Se contacts and the resulting *I-V* characteristics. Most researchers have claimed to observe steady state dark currents and interpreted the observed dark *I-V* characteristics in terms of space charge limited currents (SCLC) and even obtained the energy distribution of the deep traps (or deep localized states) from the shape of the SCLC *I-V* curve. In nearly all cases, the models were not rigorously tested against the expected scaling law for SCLC, $J/L \propto f(V/L^2)$, where J is the current density, V is the applied voltage, L is the sample thickness and f is any function that represents the SCLC *I-V* curve shape. More evidence against SCLCs comes from several sources. Pfister and Lakatos [21] found that SCLC could only be obtained by intensely illuminating one or both of the contacts with strongly absorbed (λ = 3990 Å) light. The illuminated contact is thereby made an injecting contact and the resulting steady state photocurrent vs. voltage characteristics are then indeed SCL and follow Child's law

($J \sim V^2/L^3$ for one carrier injection and $J \sim V^3/L^5$ for two carrier injection). Müller and Müller [22] reported that the dark *I-V* characteristics of Au/a-Se/Cu devices are Schottky emission limited with experimental Schottky coefficients that are within 10-20% of the theoretically expected value.

Careful study of these initial works shows several very interesting issues. First, most of the authors have mentioned that they have measured the steady state current in their samples, or that they have waited long enough for the current to stabilize. This implicitly implies that the measurements are complicated due to the presence of non-steady state (transient) currents although the authors have not mentioned this fact explicitly. Secondly, in many of the works the presence of contact "formation" process is described [23,24]. By contact "formation" the authors mean that application of high electric fields for the first time, or annealing at a temperature around 50 °C leads to permanent changes in the metal/a-Se contact properties. In some cases, the changes lead to the appearance of an ohmic region in the *I-V* curves at low voltages [23]. In other cases, the changes lead to the formation of a rectifying device [24]. Further, the authors have observed that films produced in the same run of the vacuum coater can have dark currents that can differ by more than two orders of magnitude [25].

Given the present use of a-Se in various electroded imaging device applications, in contrast to its earlier applications as xerographic photoreceptors, there is now a technological need for systematic studies of the current-voltage characteristics of various metal/a-Se/metal structures and the nature of metal contacts to a-Se. Most past papers on the *I-V* characteristics do not specify the quality of the a-Se material used, *i.e.* there is no information on the charge carrier mobilities and lifetimes to gauge whether the results are representative of device quality material.

Johanson et al. [26] studied the dark current in metal/a-Se/ITO devices with electronic (or xerographic) grade a-Se samples (good hole and electron ranges). They found that the *I-V* characteristics depend on the nature of the metal/a-Se contact and do not follow well-established models, such as Schottky emission. The existence of long transients after the application of the bias across the a-Se film has been acknowledged for the first time in this work. The dark current immediately after the application of a bias voltage to a metal/a-Se/ITO device has been observed to decay with time (in a non-exponential manner), with decay characteristics that depend on the type of metal. It has not been possible to simply correlate the dark current to the metal work function, which would be expected in the case of Schottky type of metal/a-Se contacts. Based on their data, Johanson et al. suggested that the main dominant conduction mechanism in these metal/a-Se/ITO structures was due to the injection of holes from the positive electrode rather than electrons from the negative electrode. Since, usually, the hole range $\mu_h \tau_h$ in electronic grade a-Se is much larger than the electron range $\mu_e \tau_e$, by almost an order of magnitude (Table 3), their argument seems reasonable.

There is one interesting work carried out at Xerox that should be mentioned. Tabak and Scharfe in 1970 [27] examined the shape of the transient current that follows after the application of a voltage across an a-Se film whose positive electrode side has been illuminated with light. The illumination is kept weak and the absorption depth very narrow, analogous to the conditions that are used in TOF transient photoconductivity experiments; except that TOF involves a short light pulse to generate the photocurrent. The authors observe the current shown in Fig. 3, again analogous to TOF waveforms, though the time scale is much longer. The hole transit time is 18 μs whereas the transient in Fig. 3 exhibits a transition at about 100 ms. The fall in the transient current in Fig. 3 is due to the transition of the photocurrent current from being emission limited to being space charge limited, controlled by the space charge of trapped holes in the bulk. The field is initially uniform across the sample, and the current is limited by the rate at which the holes are generated by the low-intensity light at the positive side of the sample. As holes become trapped, a space charge builds-up and modifies the internal field, and hence reduces the field at the positive side and the current eventually becomes limited by space charge.

The transition time from emission to SCLC depends on the injection rate (light intensity), and increases as the injection rate and hence the initial photocurrent decreases. A crude extrapolation of the photocurrent values down to dark current values typically observed in a-Se points to a transition tome that is over the time scale 1 – 100 seconds. Tabak and Scharfe do not consider the field dependence of the quantum efficiency, and the reduction in the injection rate as the field drops at the illuminated positive side. Nonetheless, the work is clear in identifying the fact that space charge build-up occurs in the bulk as a result of hole injection from the positive side, which modifies the internal field; and the current has a time dependence.

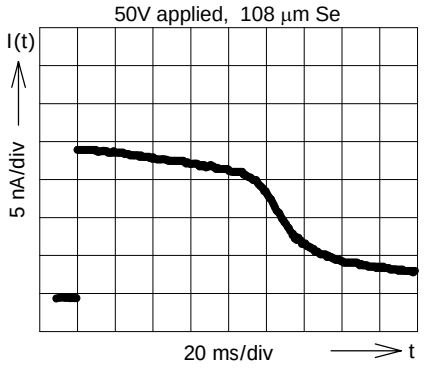

Fig. 3. The transient photocurrent under steady state weak illumination (photoinjection) right after the application of a bias voltage across an a-Se film. The positive side is illuminated. Thickness L = 108 μm, bias V = 50 V, expected TOF transit time is 18 μs, illumination wavelength is 450 nm (Data extracted from reference [27]).

The modification of the internal field due to space charge build-up also occurs in routine TOF experiments when those experiments are carried out in a repetitive mode [28,29]. There is a marked change in the shape of the TOF transient photocurrent as the TOF measurements are repeated one after another without allowing the trapped charges to be detrapped. Trapped holes modify the internal field, which affects the TOF photocurrent shape. For example, if the space charge is due to uniformly trapped holes in the bulk, then the TOF hole photocurrent decays exponentially with a time constant that depends on the space charge density [30]. The photocurrent shape itself can be used to deconvolute the space charge density $\rho(x)$ variation across the a-Se film, as shown at Xerox [31, 32].

The lack of sufficient experimental data about the dark currents in metal/a-Se/metal devices and the importance of the problem have motivated us to collect experimental data on the subject. One of the major objectives of this paper is to describe the main experimental results from that study. In this paper we also report new dark current measurements on a variety of a-Se samples and device structures.

5. Recent dark current experiments

5.1 Experimental technique and general observations

In an effort to understand and reduce the dark current in metal/a-Se/metal structures, we have re-examined the dark current by measuring the dark current vs time behaviour from the instant the voltage is applied across the device. The measurements were automated and involved applying a voltage from a programmable high stability voltage source (Stanford Research Systems, PS350 Model HV Power Supply) and measuring the current with a Keithley programmable electrometer, configured as an ammeter (Keithley, 6512 Model Programmable Electrometer) all appropriately interfaced to a computer through a GPIB. The application of the bias and the acquisition of the current as a function of time were all automated, so that the current could be accurately monitored over an extended time. In addition, various biasing schemes could also be carried out, such as well-defined step (or staircase) increases or step decreases in the applied voltage. The following observations on the current-time-voltage data are noteworthy.

(i) Generally the dark current decays with time from the instant the voltage is applied to the device. The I_d vs. t characteristics can be quite complicated, and can be fitted to a stretched exponential type of behaviour, as well as to a power law dependence on time, over a long time scale.

(i) Generally the dark current vs voltage characteristics at a given time after the bias application are not symmetric, even if the device has been fabricated to be symmetric, e.g. the Au/a-Se/Au *I-V* characteristics are not symmetric.

(ii) The dark current in some cases, for example when the applied bias has been reduced, can even flow in the opposite direction to the expected normal current flow for the new bias.

(iii) The dark current depends on the substrate temperature during the film deposition, *i.e* the dark current depends on the preparation conditions.

(iv) The dark current exhibits hysteresis effects in the sense that the *I-V* characteristics at a certain time after the application of the bias depends on the measurement history; *i.e.* the *I-V* characteristics depend on whether V is being increased or decreased.

(v) The dark current I_d before X-ray generation, and the dark current I_d' after the cessation of X-ray generation, are not the same. In general, I_d' is larger than I_d, and also decays with time. Over the time scale of the observations, I_d' did not seem to come down to the same level I_d. It is important to emphasize the problems associated with dark currents in a-Se films. It is well known in detector design that if one measures the dark current, and its effect, before irradiation then one can, in principle, subtract the effect of the dark current from the "total signal" to obtain the "actual signal". However, the dark current correction can only be done if the latter does not change with the signal (irradiation) itself. Our measurements show that there is a significant increase in the dark current following exposure to X-rays, which means that dark current corrections cannot be done accurately in a-Se detectors.

(vi) Time-of-Flight (TOF) small signal hole photocurrent probing of the sample, along the lines used at Xerox and cited above, while under a dc bias indicates that there is a substantial space charge build-up in the bulk of the sample. The initial field is uniform but as time progresses, the filed becomes non-uniform, confirming Tabak and Scharfe's early work on space charge build-up. The exact distribution of the net space charge $\rho(x)$ and its polarity across the film thickness is currently under study.

5.2. I-t and *I-V* characteristics and the reduction of the dark current

In the following, we only present selected results that have been chosen for their scientific and technological significance. These results have eventually lead to the development of the double layer a-Se X-ray detector mentioned in the introduction.

The first and foremost result, as mentioned above, is that nearly in all cases the dark current decays with time. Fig. 4 shows some typical examples of *I-t* behaviour at various applied voltages for a 130 μm stabilized a-Se film that has the Au/a-Se/Au structure. The preparation conditions and the hole and electron lifetimes are given in the figure caption. It is clear that the dark current decays significantly, by a factor of 10 - 10^2, over a time scale of 1000 s.

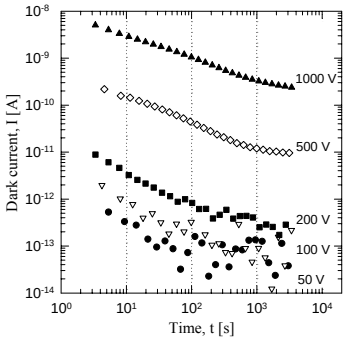

Fig. 4. Dark current I-t curves for a stabilized a-Se film deposited at 70 °C substrate temperature from an a-Se:0.3%As alloy. The sample has a thickness of 130 μm and both bottom and top contacts are Au. $\tau_h \approx 15$ μs and $\tau_h \approx 400$ μs.

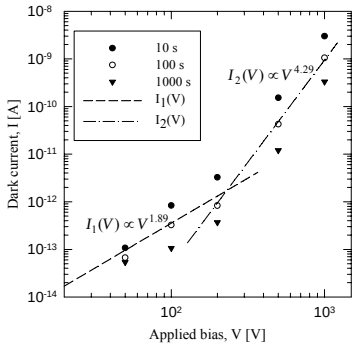

Fig. 5. Dark I-V curves constructed by taking cuts in the I-t curves at certain times at 10 s, 100 s and 1000 s, for an Au/a-Se/Au film that has the film properties stated in Fig. 4.

Dark *I-V* curves constructed by taking cuts in the *I-t* curves at certain times at 10 s, 100 s and 1000 s, are shown in Fig. 5. There appear to be two $I \propto V^n$ regions where for low voltages $n \approx 2$ and for high voltages $n \approx 4$. There seems to be no apparent ohmic region. These results are typical. For various metal/a-Se/metal structures we have found the *I-V* curves constructed from snap shot cuts on the *I-t* curves to follow $I \propto V^n$ type of behaviour. In some cases there are two regions as in Fig. 5, whereas in other cases, there is only one $I \propto V^n$ region over whole current range measured. These results are similar to those reported by Johanson et al. in 1998 [26]. These authors, however, did not investigate the effect of the substrate temperature on the dark current. Given that the substrate temperature has a dramatic effect on the hole range, which can drop by one or two orders of magnitude by lowering the substrate temperature, one would expect the dark current to show a dependence on the substrate temperature.

Fig. 6 compares the dark current density vs. the nominal applied field ($F = V/L$) characteristics observed for stabilized a-Se films prepared by hot and cold deposition. The device structure corresponds to Au/a-Se/Al/glass in which the top Au electrode is sputtered, and the a-Se is deposited onto a glass substrate that has an Al electrode. The cold deposited film corresponds to a substrate temperature $T_{\text{substrate}}$ of 25 °C, below the glass transition temperature ($T_g \approx 50$ °C) of the film material. Following cold deposition, the a-Se film is annealed near T_g. for 1 h. For the hot deposited film, $T_{\text{substrate}}$ of 70 °C > T_g.

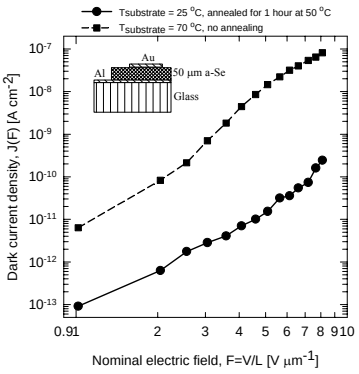

Fig. 6. Comparison of the dark current J vs. F curves for stabilized a-Se (Se:0.5%As) samples produced on hot and cold substrates under negative bias applied to the Au electrode.

It is apparent that there is a very large difference between the dark currents in the two samples in Fig. 6. The dark current in the cold deposited a-Se film is *two orders* of magnitude smaller than that in the hot deposited film. The cold deposited film traps holes *i.e.* has short hole ranges, but has good electron transport as reported previously. We believe that the large drop in the dark current is due to a large reduction in the hole component of the dark current. The dark *I-V* characteristics are *not* symmetric, as highlighted in Fig. 7. The dark current in the Au/a-Se/Al device is much smaller when the top (Au) electrode is biased negatively rather than positively.

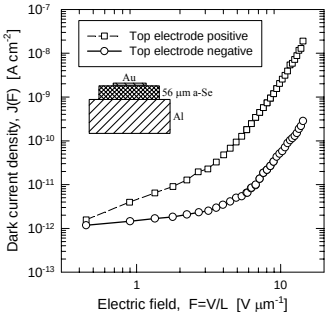

Fig. 7. Typical dependence of the dark current density J on the applied electric field F in stabilized a-Se (Se:0.5%As) films produced by deposition on a "cold " ($T_{substrate}$ = 25 °C < T_g) Al substrate. The film was annealed after the deposition at a temperature around T_g (1 hour, at ~50 °C). The top electrode (Au) was sputtered onto the surface of the annealed film.

Holes in the cold deposited a-Se film are trapped heavily and cannot contribute significantly to the dark current. By the same token, since cold deposited films have $\mu_e \tau_e > \mu_h \tau_h$, as reported previously, we would expect the dark current to depend on electron injection from the negative electrode.

Fig. 8 shows the dark current density vs. time behaviour for three different metals (Al, Au and Pt) used for the negative electrode to cold deposited a-Se films. The nominal applied field ($F = V/L$) is 10 V μm^{-1}, which is a typical operating field for a-Se X-ray photoconductors. As in other cases, the current decays with time, and the device with the Pt electrode has the lowest dark current.

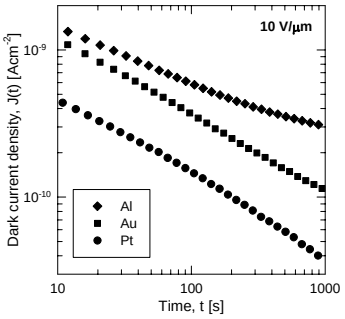

Fig. 8. The influence of the top electrode metal on the dark current J–t curves in Al/a-Se/metal structures under negative bias. The stabilized a-Se (Se:0.5%As) film is deposited on a Al/glass substrate kept at 25 °C. After mild annealing (50 °C, one hour), Pt, Au and Al were deposited onto the surface. The area of the contacts was 0.25 cm^2.

There is a reasonable correlation with the metal work function in the sense that as the work function increases from Al (Φ = 4.3 eV) to Au (Φ = 5.1 eV) to Pt (Φ = 5.7 eV), the current becomes smaller, as apparent in Fig. 8. After 100 s of bias, the dark current density is of the order of ~10^{-10} A cm^{-2} or 1 pA mm^{-2}, at a level that is more than acceptable for use as an X-ray photoconductor. While the dark current is sufficiently low, there is a trade off. The film has poor hole transport; but it does have good electron transport. As discussed below, the results in Fig. 8 provide a means of fabricating a detector structure that has very low dark currents.

6. A double layer X-ray detector structure

The reduction of the dark current in a cold deposited a-Se films provides a means of designing a novel X-ray detector structure which can be used for X-ray imaging applications under a negative bias, that is, the radiation receiving electrode is negatively biased. Fig. 9 illustrates the basic structure of the double layer structure. In general terms, first, a thin *n*-layer of thickness 5 – 20 μm of a-Se film is cold deposited onto the desired substrate. The thickness of the *n*-layer depends on the X-ray imaging technique to be used. For the dark current test sample, we simply used an Al substrate, but later we used a CCD chip to enable the construction of a practical image sensor. The thin film is then annealed at its T_g for 1 h. The *n*-layer serves as a blocking layer. The *i*-layer that serves as the photogeneration and charge transport layer is then deposited onto the *n*-layer at a substrate temperature of about 40 °C, which is close to T_g. The *i*-layer is about 100-150 μm in thickness for mammography for which the attenuation depth δ is about 50 μm. The top Pt contact is sputtered onto the *i*-layer. The device carries a negative bias on the radiation receiving electrode, which means that the hole injection is "blocked" by the *n*-layer, and the dark current is limited primarily by electron injection from the Pt contact. A similar double layer has been also fabricated on a CCD imaging chip, whose imaging properties are described below.

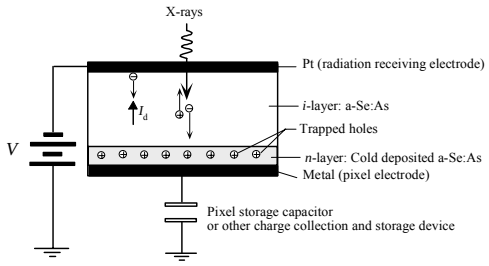

Fig. 9. Double layer a-Se X-ray detector structure with reduced dark currents. The n-layer is fabricated by cold deposition and then by annealing.

Dark current density vs. applied (nominal) field, *J* vs. *F*, characteristics of single and double layer a-Se structures are compared in Fig. 10. The currents are measured at 300 s after the application of the bias voltage. The devices are based on the Pt/a-Se/Al structures produced from amorphous selenium alloys that contained no Cl. Under negative bias operation, it is important to ensure that the electrons have long ranges, which means that halogen doping should be avoided. The single *i*-layer was deposited on a heated substrate ($T_{substrate}$ = 60 °C) from a Se-0.5%As alloy, which resulted in $\tau_h \sim 80$ μs and $\tau_e \sim 400$ μs for the *i*-layer. This single layer exhibits dark current densities that are 2-3 orders of magnitude greater than ~10^{-10} A cm^{-2} that is needed in detector applications over operating fields greater than 5 Vμm^{-1}. Fig. 10 also shows the *J*-*E* data points for a single *n*-layer produced from the same alloy (Se-0.5%As) as the hot deposited layer, but in this case $T_{substrate}$ = 25 °C. The hole and electron lifetimes in this layer were measured to be $_h$ ~ 0.8 μs and τ_h ~ 300 μs respectively, and clearly $\mu_e \tau_e >> \mu_h \tau_h$. The *J*-*E* data for a double layer *n*-*i* detector structure are also shown in Fig. 10. This particular detector structure was recently used in prototype detectors for high-resolution mammography based on the slot scanning imaging technique. [5]. Both layers in the latter structure were produced from the *same* Se-0.2%As alloy. The *n*-layer was deposited at a substrate temperature of $T_{substrate}$ = 7 °C and is 20 μm thick. The *i*-layer was deposited at a substrate temperature $T_{substrate}$ = 40 °C and is 110 μm thick. The *n*-layer in this structure has a hole lifetime $\tau_h \leq 0.6$ μs and τ_e ~ 300 μs. The lifetimes

measured in the *i*-layer were $\tau_h \sim 6$ μs and $\tau_e \sim 400$ μs. It is clear from Fig. 10 that the dark current density in the double layer *n-i* structure at 10 V/μm is almost an order magnitude lower than the one in the simple cold deposited *n*-layer. The dark current densities in *n-i* devices produced in the manner described above are somewhat lower than the typical values reported for practical *pin* structures at the same field (hatched area in Fig. 10). The smallest X-ray exposures of interest for mammography will produce current densities that are slightly higher than those corresponding to the upper end of the hatched area in Fig. 10 if the thickness of the a-Se photoconductor is about 200 μm and the applied field is larger than 5 V μm^{-1}.

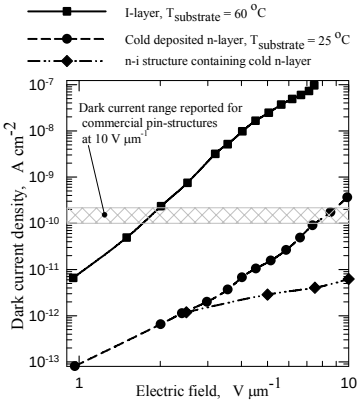

Fig. 10. Current density vs. electric field characteristics of three different a-Se based detector structures, all fabricated from stabilized a-Se (Se:0.5%As). ■ Al/a-Se/Pt structure with $T_{substrate}$ = 60 °C, which is an i-layer. ● An n-layer produced from the same alloy (Se:0.5%As) by cold deposition in which $T_{substrate}$ = 25 °C. ♦ An n-i structure. Both layers are produced from the same stabilized a-Se alloy (Se:0.2%As). The n-layer was deposited at $T_{substrate}$ = 7 °C and is 20 μm thick. The i-layer was deposited with $T_{substrate}$ = 40 °C and is 110 μm thick.

As described above, the newly proposed technology for dark current minimization limits the dark currents densities in a-Se multilayered structures to approximately the same levels as achieved by the previously existing methods. In addition, the new technology has certain potential advantages. It enables X-ray imaging with a single layer a-Se photoconductor up to electric fields of 5 Vμm^{-1} and slightly higher, which is a distinct advantage for applications in very high-resolution X-ray image detectors. The new technology is simpler for implementation than the deposition of *pin* structures from two or more boats. All the layers can be produced from the same starting a-Se alloy, and thus a simple single boat evaporation process can be used. The cold deposition technology avoids the necessity to produce the doped materials required for the production of *n*- and *p*-layers in the *pin* structure. It is important to emphasize that the advantages offered by the new technology are much more pronounced when the radiation-receiving electrode is negatively biased. This is the case for many detector applications, because the image readout electronic circuit offers distinct advantages in simplicity and price when designed to collect electrons, which requires the use of a negatively biased photoconductor (radiation receiving electrode is negative).

The double layer detector structure in Fig. 9 was used on top of a specially designed charged coupled device called the SALLY CCD. The CCD detector is suitable for slot scanning X-ray imaging, and utilizes the time delayed integration readout technique. The photograph of the a-Se based CCD X-ray detector is shown in Fig. 11. The detector is mounted in a ceramic chip carrier and wire bonded. The PCB card on which the chip carrier is mounted provides a means to conveniently connect the X-ray detector to the data acquisition and cooling systems. The latter wire is glued to the radiation receiving electrode of the detector by conducting epoxy.

Fig. 12 shows the X-ray image of a printed circuit board (PCB) with the holes and the metal traces (on the left) and an image of an apple seed obtained using the a-Se CCD detector in Fig. 11. Both images are obtained with the energy of the X-rays in the mammography range.

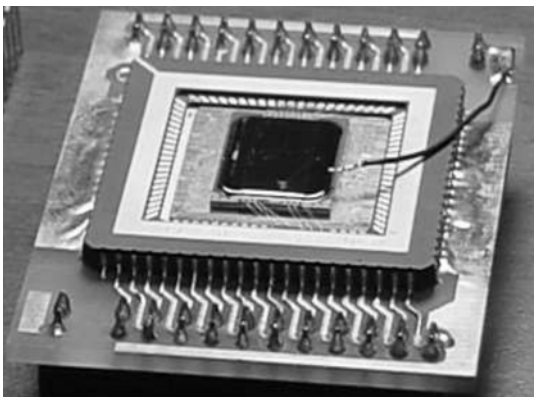

Fig. 11. A prototype X-ray detector based on a SALLY CCD and an a-Se photoconductor layer produced by the cold deposition technology described in this work.

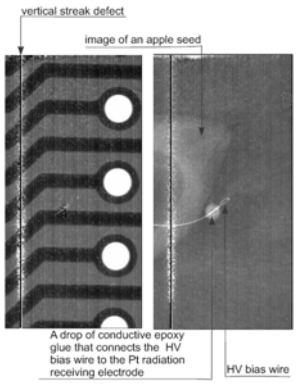

Fig. 12. X-ray images of a printed circuit board (PCB) with the holes and the metal traces (left) and a partial image of an apple seed (right). The CCD has a vertical streak defect. The HV bias wire and the epoxy glue holding it to the top contact are also visible. (Image courtesy of David Hunter, Sunnybrook and Women's Hospital, Toronto.)

Fig. 13 presents X-ray images of small areas of resolution phantoms taken with the a-Se CCD detector. The imaged line pattern areas have spatial frequencies of 5 and 16 lines mm^{-1}. (More were imaged, but are not shown). Since the lines in all the images can be clearly distinguished, the experiment confirms that the spatial resolution of the a-Se SALLY detector is better than 16 lines mm^{-1}.

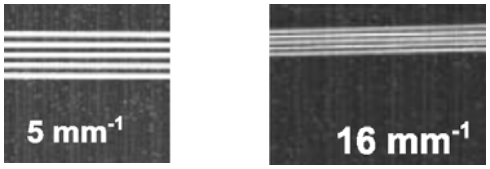

Fig. 13. Differently scaled X-ray images of a resolution bar phantom that show that the a-Se SALLY CCD X-ray detector can resolve better than 16 lines per mm.

Acknowledgements

The authors would like to thank the National Institute of Health (USA) and Sunnybrook Health Sciences Centre, Toronto, for financial support. We are most grateful to David Hunter at Sunnybrook for providing the X-ray images taken with the a-Se SALLY CCD detector.

References

[1] J. A. Rowlands, J. Yorkston, in Handbook of Medical Imaging, Ed. J. Beutel, H. L. Kundel and R. L. Van Metter, SPIE Press, Washington (2000), Vol. **1**, Ch. 4.
[2] S. O. Kasap, J. A. Rowlands, Proc. of IEEE **90**, 591 (2002).
[3] B. Polischuk, Z. Shukri, A. Legros, H. Rougeot, SPIE Proc. **3336,** 494 (1998).
[4] D. C. Hunt, O. Tousignant, J. A. Rowlands, Med. Phys. **31,** 1166 (2004).
[5] D. M. Hunter, G. Belev, G. DeCrescenzo, S. Kasap, J. G. Mainprize, G. Mawdsley, J. A. Rowlands, C. Smith, T. Tümer, V. Verpakhovski, Shi Yin, M. J. Yaffe, SPIE Proc. **5368**, 466 (2004).
[6] M. A. Abkowitz, Philos. Mag. Lett. **58**, 53 (1988).
[7] M. Abkowitz, J. M. Markovics, Solid State Commun. **44**, 1431 (1982) .
[8] S. O. Kasap, B. Polischuk, M. A. Abkowitz, Phil. Mag. Lett. **62**, 377 (1990).
[9] B. Polischuk, S. O. Kasap, V. Aiyah, A. Baillie, M. A. Abkowitz, Can. J. of Phys. **69**, 361 (1991).
[10] K. Hecht, Z. Physik **77**, 235 (1932).
[11] Y. Nemirovsky, A. Ruzin, G. Asa, J. Gorelik, J. Electron. Mater. **25**, 1221 (1996).
[12] S. O. Kasap, J. Phys. D: Appl. Phys. **33**, 2853 (2000).
[13] M. Z. Kabir, S. O. Kasap, Appl. Phys. Lett. **80,** 1664 (2002).
[14] J. R. Pierce, Proc IRE **44**, 601 (1956).
[15] S. O. Kasap, Principles of Electronic Materials and Devices, 3rd Edition, McGraw-Hill (2006), Ch. 1.
[16] J. Hynecek, IEEE Trans. Electron Devices **37**, 640 (1990).
[17] R. A. Street, K. Shah, S. Ready, R. Abe, P. Bennet, M. Klugerman, Y. Dmitriyev, SPIE Proc. **3336**, 24 (1998).
[18] M. Z. Kabir, S. O. Kasap, J. A. Rowlands, in Springer Handbook of Electronic and Photonic Materials, Ed. Safa Kasap and Peter Capper, Springer, Heidelberg (2006), Ch. 48.
[19] G. Belev, S. O. Kasap, J. Non-Cryst Solids **345,** 484 (2004).
[20] S. O. Kasap, K. V. Koughia, B. Fogal, G. Belev, R. E. Johanson, Semiconductors **37,** 816 (2003).
[21] G. Pfister, A. I. Lakatos, Phys. Rev. **B 6**, 3012 (1972).
[22] L. Müller, M. Müller, J. Non-Cryst. Solids **4**, 504 (1970).
[23] H. P. D. Lanyon, Phys. Rev. **130**, 134 (1963).
[24] S. Touihri, G. Safoula, J. C. Bernède, Phys. Stat. Sol. A **159**, 569 (1997)
[25] G. Pfister, A. I. Lakatos, Phys. Rev. B **6**, 3012 (1972).
[26] R. E. Johanson, S. O. Kasap, B. Polischuk, J. A. Rowlands, J. Non-Cryst. Solids **227**, 1359 (1998).
[27] M. Tabak, M. Scharfe, J. Appl Phys. **41**, 2114 (1970).
[28] B. Polischuk, S. O. Kasap, D. Dodds, S. Yannacopoulos, Proc. 4-th Intern. Symp. on the Uses of Se and Te, Ed. S. Carapella Jr. Selenium-Tellurium Development Association, Darien, CT, 1989, p. 202.
[29] H. Pinsler, Proc. 4-th Intern. Symp. on the Uses of Se and Te, Ed. by S. Carapella Jr., Selenium-Tellurium Development Association, Darien, CT, 1989, p.130
[30] M. Scharfe, M. Tabak, J. Appl. Phys**. 40**, 3230 (1969).
[31] S. B. Berger, R. C. Enck, M. E. Scharfe, B. E. Springer, in Physics of Selenium and Tellurium, ed. E. Gerlach and P. Grosse, Springer-Verlag, New York (1979), p.256.
[32] S. B. Berger, R. C. Enck, Proc. 2nd Intern. Symp. on Industrial Uses of Se and Te, Toronto, Canada, 1980, p.179.

*Corresponding author: safa.kasap@.usask.ca